

An *ab initio* recipe for taming nuclear-structure dependence of V_{ud} : the $^{10}\text{C} \rightarrow ^{10}\text{B}$ superallowed transition

Michael Gennari^{1,2}, Mehdi Drissi¹, Mikhail Gorchtein^{3,4}, Petr Navrátil^{1,2}, and Chien-Yeah Seng^{5,6}

¹TRIUMF, 4004 Wesbrook Mall, Vancouver, BC V6T 2A3, Canada

²University of Victoria, 3800 Finnerty Road, Victoria, British Columbia V8P 5C2, Canada

³Institut für Kernphysik, Johannes Gutenberg-Universität Mainz, 55128 Mainz, Germany

⁴PRISMA⁺ Cluster of Excellence, Johannes Gutenberg-Universität Mainz, 55128 Mainz, Germany

⁵Facility for Rare Isotope Beams, Michigan State University, East Lansing, MI 48824, USA and

⁶Department of Physics, University of Washington, Seattle, WA 98195-1560, USA

(Dated: May 30, 2024)

We report the first *ab initio* calculation of the nuclear-structure-dependent radiative correction δ_{NS} to the $^{10}\text{C} \rightarrow ^{10}\text{B}$ superallowed transition, computed with the no-core shell model and chiral effective field theory. We obtain $\delta_{\text{NS}} = -0.400(29)_{\text{nuc}}(12)_{n,\text{el}}$ with a 1.7-times reduction in the nuclear uncertainty when compared to the current literature estimate based on the shell model and Fermi gas picture. This work paves the way for a precise determination of V_{ud} from superallowed beta decays.

Unitarity of the Cabibbo-Kobayashi-Maskawa (CKM) quark-mixing matrix [1, 2] implies for its top-row elements, $\Delta_u \equiv |V_{ud}|^2 + |V_{us}|^2 + |V_{ub}|^2 - 1 = 0$. Given the experimental accuracy of these elements, the top-row CKM unitarity constraint provides an important avenue for testing the Standard Model (SM) and its extensions at low energies. A revived interest of this topic follows the recent observation of an apparent unitarity violation at $\sim 3\sigma$: $\Delta_u = -1.48(53) \times 10^{-3}$ [3]. Given its high impact on the search for new physics [4–16], all ingredients underlying this anomaly have to be carefully scrutinized.

From ^{10}C to ^{74}Rb , the 23 measured superallowed beta transitions of $T(J^P) = 1(0^+)$ nuclei combine to provide currently the most accurate extraction of V_{ud} , the largest top-row CKM matrix element. This extraction relies on inputs from theory as much as on experimental measurements, as summarized by the following master formula [17]

$$|V_{ud}|_{0^+}^2 = \frac{\mathcal{K}}{ft(1 + \delta'_R)(1 + \Delta_R^V)(1 + \delta_{\text{NS}} - \delta_C)}, \quad (1)$$

where $\mathcal{K} = \pi^3 \ln 2 / G_F^2 m_e^5$ and the quantities δ'_R , Δ_R^V , δ_{NS} and δ_C represent SM corrections that must be computed to an absolute precision of 10^{-4} to further probe the current CKM unitarity tension. Among them, Δ_R^V and δ_{NS} entail the effects of the hadron/nuclear-structure dependent electromagnetic radiative corrections (RC). Recent studies based on dispersion relations and lattice Quantum Chromodynamics (QCD) have largely pinned down the single-nucleon RC Δ_R^V [18–23]. This shifted the attention to δ_{NS} , the nucleus-dependent part of the RC, which

has traditionally been evaluated with the nuclear shell model [24–27]. It has to be noted that splitting the full RC into the three separate pieces requires a separation of scales pertinent to Quantum Electrodynamics (QED), hadron and nuclear dynamics. Recent studies in the dispersion relation framework [18, 28] indicated that the previously assumed scale separation was flawed. This finding led to an increased uncertainty in δ_{NS} which makes it currently the largest source of error in $|V_{ud}|_{0^+}$: $|V_{ud}|_{0^+} = 0.97361(5)_{\text{exp}}(6)_{\delta'_R}(4)_{\delta_C}(28)_{\delta_{\text{NS}}}(10)_{\Delta_R^V}$ [29]. Hence, the reduction of the δ_{NS} uncertainty with *ab initio* nuclear many-body methods is among the most urgent tasks for the precision test of the first-row CKM unitarity. In this Letter we report the first complete study of such kin, focusing on the ^{10}C superallowed beta decay.

The key hadronic ingredient to the nucleus-independent and nucleus-dependent RCs, Δ_R^V and δ_{NS} , is the γW -box contribution with

$$\Delta_R^V + \delta_{\text{NS}} = 2 \square_{\gamma W}^{b,\text{nuc}} + \dots, \quad (2)$$

where $\square_{\gamma W}^b(E_e)$ is given in Eq. (3) with associated Feynman graph in Fig. S 1, the nuclear correction is given by $\delta_{\text{NS}} = 2(\square_{\gamma W}^{b,\text{nuc}} - \square_{\gamma W}^{b,n})$ and the ellipses stand for known terms not related to the γW -box [29, 30]. All hadronic physics entering the γW -box does so via the invariant amplitude T_3 , itself derived from a generalized Compton scattering amplitude involving electromagnetic and axial charged weak currents. Explicitly, the $\square_{\gamma W}^b(E_e)$ and Compton amplitude T_3 read

$$\square_{\gamma W}^b(E_e) = -e^2 \int \frac{d^4 q}{(2\pi)^4} \frac{M_W^2}{M_W^2 - q^2} \frac{1}{q^2 + i\varepsilon} \frac{1}{(p_e - q)^2 - m_e^2 + i\varepsilon} \left[q^2 - p \cdot q \frac{(p \cdot q)m_e^2 - (p_e \cdot q)(p \cdot p_e)}{M^2 m_e^2 - (p \cdot p_e)^2} \right] \frac{T_3(\nu, \mathbf{q})}{(p \cdot q) f_+} \quad (3)$$

$$T_3(\nu, \mathbf{q}) = 4\pi i \frac{\nu}{\mathbf{q}} \sqrt{M_i M_f} \sum_{J=1}^{\infty} (2J+1) \langle \Psi_f | \left\{ T_{J0}^{\text{mag.}} (z_f - H)^{-1} T_{J0}^{5,\text{el.}} + T_{J0}^{\text{el.}} (z_f - H)^{-1} T_{J0}^{5,\text{mag.}} \right. \\ \left. + T_{J0}^{5,\text{mag.}} (z_i - H)^{-1} T_{J0}^{\text{el.}} + T_{J0}^{5,\text{el.}} (z_i - H)^{-1} T_{J0}^{\text{mag.}} \right\} (\mathbf{q}) | \Psi_i \rangle . \quad (4)$$

These expressions depend on (i) the on-shell electron 4-momentum p_e (ii) the virtual gauge boson 4-momentum q with $\nu = q_0$, $\mathbf{q} = |\vec{q}|$, $z_i = M_i - \nu + i\epsilon$ and $z_f = M_f + \nu + i\epsilon$ (iii) the tree-level Fermi matrix element f_+ and (iv) the rest frame 4-momentum of the nucleus, taken in the forward limit such that $p \approx p_i \approx p_f$ up to differences in the nuclear masses. To facilitate the use of the nuclear many-body theory, a non-relativistic reduction of the SM current operators to the effective one-body nucleonic operators [31–33] has been made by expressing the Compton amplitude in terms of the nuclear resolvent and performing a multipole expansion of the currents [29, 34]. This formalism has been used extensively in nuclear theory to compute electromagnetic and weak transitions, e.g., see Refs. [35–37]. We then arrive at the expression for T_3 given in Eq. (4) which further depends on (i) the multipole operators (ii) the nuclear Hamiltonian $H = H_{\text{intrinsic}} + H_{\text{c.m.}}$ and (iii) the non-relativistic $J^P = 0^+$ nuclear states $|\Psi_i\rangle$ and $|\Psi_f\rangle$. Our conventions are consistent with the non-relativistic electroweak operator basis defined in Refs. [32, 33] and expressions for the multipole operators may be found in the Supplemental Material.

Pragmatic evaluation of T_3 requires special attention as the resolvents, when integrated over the loop 4-momentum in Eq. (3), traverse an infinite number of singularities in the discrete and continuum spectrum. Circumnavigating the vast majority is possible via Wick rotation, yet, care is required in applying Cauchy’s theorem since several poles in the ν -integral cross in and out of the Wick contour, as illustrated in Fig. 1. Such poles may be classified into two categories: those in the electron propagator labelled by the set $P_e^{(+)}$ and a subset of poles in the nuclear spectrum which involve transitions to intermediate bound states lying *below* the final nuclear state, labelled by the set $P_{\mathcal{N}}^{(-)}$. Applying the contour deformation and accounting for incurred residue contributions, we find that

$$\square_{\gamma W}^b = (\square_{\gamma W}^b)_{\text{Wick}} + (\square_{\gamma W}^b)_{\text{res},e} + (\square_{\gamma W}^b)_{\text{res},T_3} , \quad (5)$$

where the effect of the deformation reduces to the contribution along the Γ_{Wick} contour. As the Wick and electron residue terms are regular as $E_e \rightarrow 0$, for simplicity, we expand them to leading order in the electron energy. Overall, this leads to an $\mathcal{O}(E_e)$ evaluation given by

$$\square_{\gamma W}^b(E_e) = \boxplus_0 + \boxplus_1 E_e + (\square_{\gamma W}^b)_{\text{res},T_3}(E_e) + \mathcal{O}(E_e^2) . \quad (6)$$

Expressions for each term on the right-hand-side can be found in Ref. [29] as well as in the Supplementary

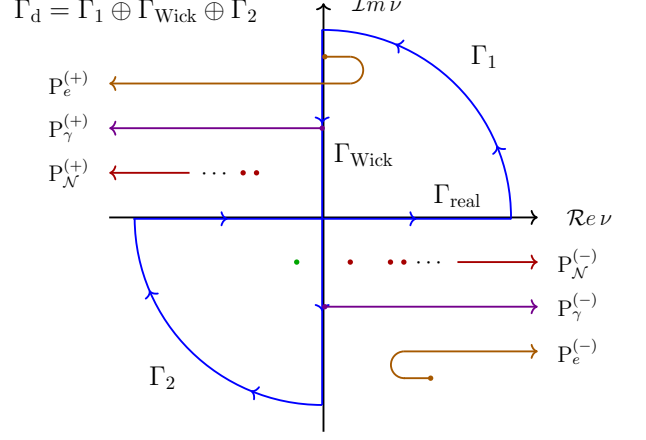


Figure 1: Example trajectories of the ν -integral poles in Eq. (3) coming from the (i) nuclear propagators in T_3 (ii) photon propagator and (iii) electron propagator, with sets labelled by \mathcal{N} , γ and e , respectively.

Material. Analysis of the $\square_{\gamma W}^b(E_e)$ function requires a nuclear theory evaluation of T_3 for which we apply the *ab initio* no-core shell model (NCSM) [38].

In the NCSM, nuclei are considered to be systems of A non-relativistic point-like nucleons interacting via realistic chiral Effective Field Theory (χ EFT) two-nucleon (NN) and three-nucleon (3N) interactions which serve as the sole input to the approach. Each nucleon is an active degree of freedom and the Galilean invariance of observables, as well as nuclear spin and parity, are conserved. The many-body eigenstates are expanded over a basis of antisymmetric A -nucleon harmonic oscillator (HO) states parameterized by the oscillator frequency Ω and containing states with excitations of quanta up to $N_{\text{max}} \hbar \Omega$ above the lowest Pauli configuration. The NCSM spectrum then contains both the bound discrete spectrum and a discretization of the continuum spectrum.

In this work, we apply two interactions derived in the χ EFT framework. At the two-body level, we use the NN–N⁴LO(500) [39] interaction across the board, whereas at the three-body level we apply the (a) 3N_{lml} interaction [40] and (b) 3N_{lml}^* interaction [41]. The latter contains an additional sub-leading contact (E_7) enhancing spin-orbit strength [42]. To accelerate convergence with respect to the size of the many-body configuration space, the chiral interactions are softened via Similarity Renormalization Group (SRG) [43]. Presently, we use the evolution parameters of $\lambda_{\text{SRG}} = 1.8 \text{ fm}^{-1}$ and $\lambda_{\text{SRG}} = 2.0 \text{ fm}^{-1}$ for}

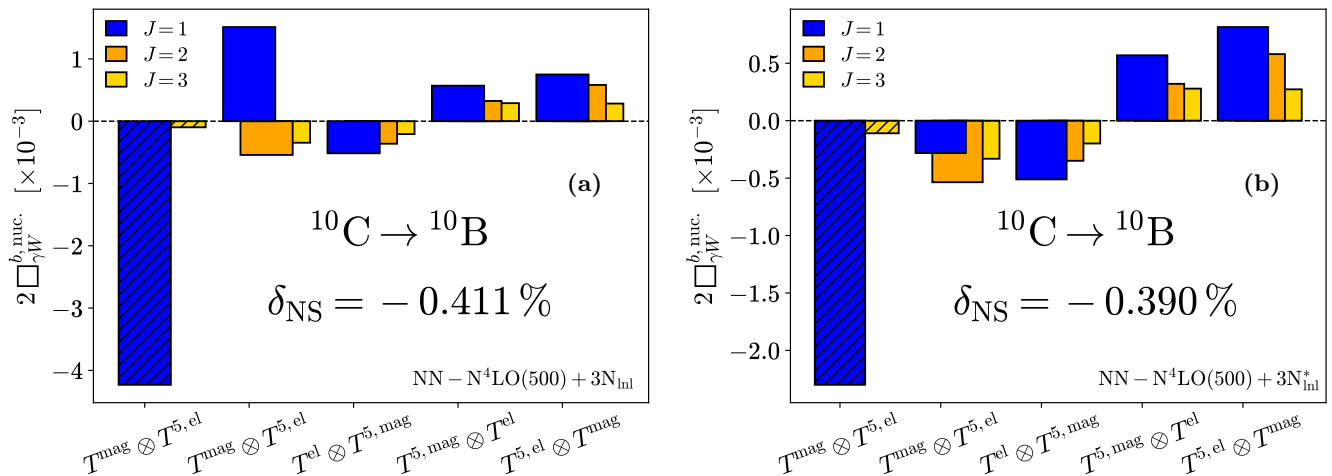


Figure 2: Breakdown of the $\Box_{\gamma W}^{b,\text{nuc}}$ into (i) different electroweak operator structures in the Compton amplitude and (ii) each moment in the multipole expansion, obtained with (a) the chiral NN-N⁴LO(500)+3N_{lnl} and (b) NN-N⁴LO(500)+3N_{lnl}^{*} interactions, in the NCSM. Residue contributions and contributions from the electron energy expansion are shown as hatched and solid bars, respectively.

the NN-N⁴LO(500)+3N_{lnl} and NN-N⁴LO(500)+3N_{lnl}^{*} interactions, respectively. To gauge convergence, model spaces up to $N_{\text{max}} = 7$ with oscillator frequencies in the range of $\hbar\Omega = 16-20$ MeV have been applied.

Employing the NCSM with χ EFT Hamiltonians in the evaluation of T_3 requires us to compute the resolvent amplitudes up to intermediate 3-momentum transfer ($\mathbf{q} \lesssim 500$ MeV). A naïve calculation is computationally infeasible, yet, via subspace techniques such as the Lanczos strength method [44–46], the complexity may be reduced to solving the many-body Schrödinger equation with a source term, i.e., $(z - H)|\Psi_n\rangle = O_{JM}|\Psi_i\rangle$. This approach was previously explored in NCSM evaluations of anapole and electric dipole moments [47, 48]. In our case, O_{JM} corresponds to any of the operators acting on the initial state in Eq. (4) and $\{\Psi_n\}$ denotes the set of intermediate excited states; these are confined to a subspace of the Hamiltonian characterized by the representation of the source vector $O_{JM}|\Psi_i\rangle$. Remarkably, despite the limited convergence of high-lying eigensolutions, the ν -integrals over T_3 rapidly converge with respect to the Krylov subspace truncation. This is a consequence of the exact reproduction of sum-rules when employing the Lanczos strength method [49–51].

While we are able to numerically evaluate the resolvent amplitudes to high-precision, in using χ EFT and the NCSM we are restricted in the physics which enters the resolvent itself. The *ab initio* nuclear box diagram $(\Box_{\gamma W}^{b,\text{nuc}})_{\text{ab}}$ only contains contributions from nucleonic intermediate states; any non-nucleonic or scattering physics above the pion-production threshold is beyond the reach of this approach. It is then sensible to combine $(\Box_{\gamma W}^{b,\text{nuc}})_{\text{ab}}$ with the purely nucleonic (elastic) contribution to the

single-nucleon box diagram as

$$\delta_{\text{NS}} = 2 \left\{ (\Box_{\gamma W}^{b,\text{nuc}})_{\text{ab}} - (\Box_{\gamma W}^{b,n})_{\text{el}} + \delta(\Box_{\gamma W}^{b,n})_{\text{sh}} \right\}, \quad (7)$$

where $(\Box_{\gamma W}^{b,n})_{\text{el}} = 1.06(6) \times 10^{-3}$ [30]. The last term represents contributions from energies above the pion-production threshold where the production of multi-hadron intermediate states is affected by the nuclear environment, a phenomenon referred to as “nuclear shadowing” [52, 53]. This contribution to δ_{NS} is introduced here for the first time. A precise treatment of the shadowing contribution is beyond the scope of this paper, however, we infer its size from the “inelastic” component of the single-nucleon box corrected for nuclear shadowing effects based on experimental data, giving $|\delta(\Box_{\gamma W}^{b,n})_{\text{sh}}| < 1.2 \times 10^{-4}$. Further details may be found in the Supplementary Material.

In Fig. 2 we present the first *ab initio* calculations of the nuclear structure radiative correction δ_{NS} obtained with the aforementioned chiral interactions. In each case, we show the breakdown of contributions to the $\Box_{\gamma W}^{b,\text{nuc}}$ coming from (i) different electroweak operator structures in the Compton amplitude and (ii) each moment in the multipole expansion. Interestingly, we observe a large relative size for the $J = 1$ Compton amplitude residue – shown as a hatched bar – in the total evaluation of the nuclear γW -box. As these residues involve transitions to the intermediate ^{10}B states lying below the final 0^+ excited state, i.e., they only depend on the low-lying discrete nuclear spectrum, the magnitude of the contribution can be largely attributed to the strength of $J = 1$ electromagnetic transitions between the ^{10}B excited 0^+ and lower-lying 1^+ states. Unlike the amplitudes involving in-

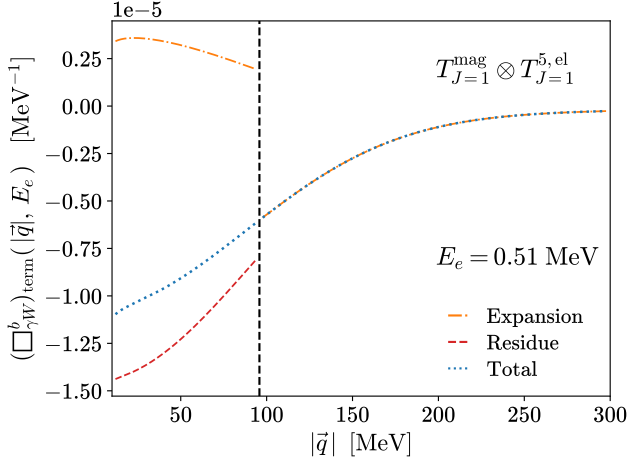


Figure 3: Slice of $T_{J=1}^{\text{mag}} \otimes T_{J=1}^{5,\text{el}}$ contribution to the γW -box integrand at $E_e \approx m_e$. The Compton residue (dashed), $\mathcal{O}(E_e)$ expansion (dash-dotted) and total sum (dotted) are as detailed in Eq. (6). The vertical dashed line corresponds to $\mathbf{q}_{\text{max}} = \sqrt{M_f^2 - M_k^2}$ where k is the lowest-lying $^{10}\text{B}(1^+)$ state.

intermediate resolvent operators, these are computationally straightforward to evaluate. However, despite the relative size of the residues being a shared feature of both calculations, we find that the distribution of strength for the $T_{J=1}^{\text{mag}} \otimes T_{J=1}^{5,\text{el}}$ amplitude into the residue and non-residue pieces is notably different. In the calculation with the NN-N⁴LO(500)+3N_{lnl} interaction, the residue represents about two-thirds of the total contribution to the $\square_{\gamma W}^{b,\text{nuc}}$. In contrast, when employing the NN-N⁴LO(500)+3N_{lnl}^{*} interaction there is a reshuffling of the amplitude strength; the residue is about half as large and the $J = 1$ moment of the non-residue contribution changes overall sign. Regardless, the predictions for δ_{NS} are largely unaffected and differ absolutely by only $\sim 2 \times 10^{-4}$. In Fig. 3, we show the decomposition of the $\square_{\gamma W}^b(E_e)$ integrand, for the $T_{J=1}^{\text{mag}} \otimes T_{J=1}^{5,\text{el}}$ amplitude, into the terms described in Eq. (6). The terms are plotted at fixed electron energy $E_e \approx m_e$ over the virtual gauge boson 3-momentum and come from the calculation with the NN-N⁴LO(500)+3N_{lnl}^{*} interaction. Pictured is the combination of the electron residue and Wick contributions calculated up to $\mathcal{O}(E_e)$, shown as dash-dotted, and the Compton residue contribution, shown as dashed, respectively labelled by *expansion* and *residue*. Despite the obvious discontinuities in the individual contributions at $\mathbf{q} = \mathbf{q}_{\text{max}}$, the sum is continuous over the 3-momentum, as expected.

In Fig. 4, we present NCSM evaluations of δ_{NS} over a range of increasing $N_{\text{max}} = 3 - 7$ configuration space sizes. Variation of the oscillator frequency characterizing the many-body basis ($\hbar\Omega$) has been performed with the

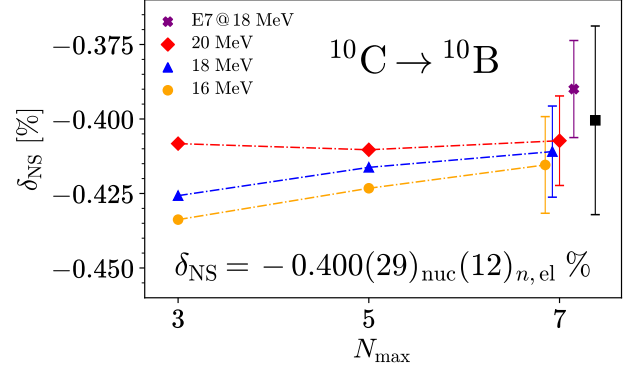


Figure 4: Sequences of δ_{NS} evaluations in the NCSM with $N_{\text{max}} = 3, 5, 7$ model space truncations and frequencies $\hbar\Omega = 16 - 20$ MeV. The E_7 point is obtained with the NN-N⁴LO(500) + 3N_{lnl}^{*} interaction; all other points are generated with the NN-N⁴LO(500) + 3N_{lnl} interaction. Error bars are as described in the text.

NN-N⁴LO(500)+3N_{lnl} interaction while a single frequency was chosen for use with the NN-N⁴LO(500) + 3N_{lnl}^{*} interaction. For brevity, we quote the uncertainties entering the δ_{NS} extractions and leave the finer details to the Supplemental Material. For a sequence of N_{max} calculations at a fixed frequency, the error bars on the final point are determined from the (i) many-body basis truncation (ii) multipole expansion truncation (iii) single-nucleon dipole form factors [18, 54] and (iv) subtraction of the elastic part of the free neutron γW -box [3, 30]. The prediction for δ_{NS} in Fig. 4 (black square) is obtained from averaging the two interaction calculations at $\hbar\Omega = 18$ MeV. The nuclear error is obtained from the quadrature combination of the partial model errors (PMEs), given by (i) – (iii), along with the errors from (v) chiral expansion truncation (vi) choice of the oscillator frequency and (vii) nuclear shadowing effects, labelled by χ , Ω and “sh”, respectively.

Thus, we predict the nuclear-structure-dependent RC to the $^{10}\text{C} \rightarrow ^{10}\text{B}$ superallowed decay rate to be

$$\delta_{\text{NS}} = -0.400(10)_{\text{PME}}(8)_{\Omega}(10)_{\chi}(24)_{\text{sh}}(12)_{n,\text{el}} \% \quad . \quad (8)$$

By construction, the uncertainty from subtraction of $(\square_{\gamma W}^{b,n})_{\text{el}}$ is totally anti-correlated to the one in the single-nucleon RC, $\Delta_R^V = 0.02479(12)_{n,\text{el}}(14)_{n,\text{inel}}(10)_{\text{hi}}$. This value is taken from Ref.[30], with errors from the elastic (el) and inelastic (inel) parts of the single-nucleon box diagram, as well as higher-order QCD+QED corrections (hi). It is hence natural to quote the full RC

$$\Delta_R^V + \delta_{\text{NS}} = 0.02079(29)_{\text{nuc}}(14)_{n,\text{inel}}(10)_{\text{hi}} \quad , \quad (9)$$

as the (n,el) uncertainty drops out in the sum. Our prediction for δ_{NS} agrees with the value $\delta_{\text{NS}} = -0.400(50)\%$ quoted in Ref. [17] with a factor of 1.7 reduction in the

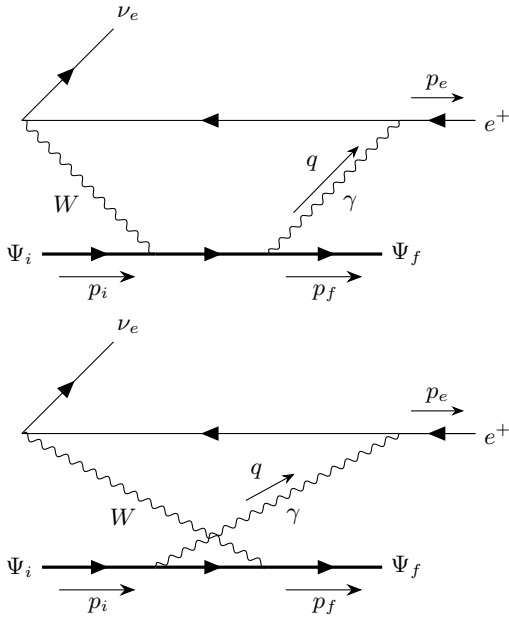
nuclear uncertainty. It further disagrees with $\delta_{\text{NS}} = -0.347(35)\%$ quoted in Ref. [55], confirming the importance of the new nuclear corrections due to quasi-elastic nucleon excitations pointed out in Refs. [18, 28].

All in all, this work provides a recipe for modern, systematically improvable calculations of general electroweak RCs in nuclei and paves the way for a more precise determination of V_{ud} . Future pathways to further improving the precision of these calculations include a deeper understanding of the EFT connection of SM processes to nucleon-level processes, the treatment of higher-body currents at the many-body level and a more sophisticated treatment of the high-energy contributions to the nuclear structure functions. In particular, follow-up studies on nuclear shadowing effects would greatly benefit the extraction of quantities like δ_{NS} which rely on electroweak physics that probes hadronic structure over vast energy scales. Additionally, as the extraction of V_{ud} is not limited to theory alone, future plans to improve theoretical precision serve as motivation for a new experimental determination of the ^{10}C branching ratio, which has historically suffered from large uncertainty. In fact, already in contemplation is a new measurement program using superconducting tunnel junctions to detect ^{10}B recoils in analogy with the successful ^7Be electron capture measurements [56–58]. Moreover, the methodology explored in this work is readily applicable to the superallowed decays of ^{14}O , ^{18}Ne and ^{22}Mg , which will be studied in follow-up works, and can be easily generalized to other electroweak processes such as parity-violating electron-nucleus scattering.

We thank Vincenzo Cirigliano, Wouter Dekens, Martin Hoferichter, Emanuele Mereghetti, Oleksandr Tomalak, Doron Gazit and Ryan Plestid for many inspiring discussions. This work was supported by the NSERC Grant No. SAPIN-2022-00019. TRIUMF receives federal funding via a contribution agreement with the National Research Council of Canada. Computing support came from an INCITE Award on the Summit and Frontier supercomputers of the Oak Ridge Leadership Computing Facility (OLCF) at ORNL and from the Digital Research Alliance of Canada. M.G. acknowledges support by EU Horizon 2020 research and innovation programme, STRONG-2020 project under grant agreement No 824093, and by the Deutsche Forschungsgemeinschaft (DFG) under the grant agreement GO 2604/3-1. The work of C.-Y.S. is supported in part by the U.S. Department of Energy (DOE), Office of Science, Office of Nuclear Physics, under the FRIB Theory Alliance award DE-SC0013617, and by the DOE grant DE-FG02-97ER41014. We acknowledge support from the DOE Topical Collaboration “Nuclear Theory for New Physics”, award No. DE-SC0023663.

-
- [1] N. Cabibbo, *Meeting of the Italian School of Physics and Weak Interactions Bologna, Italy, April 26-28, 1984*, Phys. Rev. Lett. **10**, 531 (1963).
 - [2] M. Kobayashi and T. Maskawa, Prog. Theor. Phys. **49**, 652 (1973).
 - [3] V. Cirigliano, A. Crivellin, M. Hoferichter, and M. Moulson, Phys. Lett. B **838**, 137748 (2023), arXiv:2208.11707 [hep-ph].
 - [4] B. Belfatto, R. Beradze, and Z. Berezhiani, Eur. Phys. J. C **80**, 149 (2020), arXiv:1906.02714 [hep-ph].
 - [5] Y. Grossman, E. Passemar, and S. Schacht, JHEP **07**, 068 (2020), arXiv:1911.07821 [hep-ph].
 - [6] A. Crivellin and M. Hoferichter, Phys. Rev. Lett. **125**, 111801 (2020), arXiv:2002.07184 [hep-ph].
 - [7] M. Kirk, Phys. Rev. D **103**, 035004 (2021), arXiv:2008.03261 [hep-ph].
 - [8] A. Crivellin, F. Kirk, C. A. Manzari, and M. Montull, JHEP **12**, 166 (2020), arXiv:2008.01113 [hep-ph].
 - [9] A. K. Alok, A. Dighe, S. Gangal, and J. Kumar, Phys. Rev. D **108**, 113005 (2023), arXiv:2108.05614 [hep-ph].
 - [10] A. Crivellin, M. Hoferichter, M. Kirk, C. A. Manzari, and L. Schnell, (2021), arXiv:2107.13569 [hep-ph].
 - [11] A. Crivellin, M. Kirk, T. Kitahara, and F. Mescia, JHEP **03**, 234 (2023), arXiv:2212.06862 [hep-ph].
 - [12] B. Belfatto and Z. Berezhiani, JHEP **10**, 079 (2021), arXiv:2103.05549 [hep-ph].
 - [13] B. Belfatto and S. Trifinopoulos, Phys. Rev. D **108**, 035022 (2023), arXiv:2302.14097 [hep-ph].
 - [14] V. Cirigliano, D. Díaz-Calderón, A. Falkowski, M. González-Alonso, and A. Rodríguez-Sánchez, JHEP **04**, 152 (2022), arXiv:2112.02087 [hep-ph].
 - [15] V. Cirigliano, W. Dekens, J. de Vries, E. Mereghetti, and T. Tong, (2023), arXiv:2311.00021 [hep-ph].
 - [16] M. Dawid, V. Cirigliano, and W. Dekens, (2024), arXiv:2402.06723 [hep-ph].
 - [17] J. C. Hardy and I. S. Towner, Phys. Rev. C **102**, 045501 (2020).
 - [18] C. Y. Seng, M. Gorchtein, and M. J. Ramsey-Musolf, Phys. Rev. **D100**, 013001 (2019), arXiv:1812.03352 [nucl-th].
 - [19] C.-Y. Seng, M. Gorchtein, H. H. Patel, and M. J. Ramsey-Musolf, Phys. Rev. Lett. **121**, 241804 (2018), arXiv:1807.10197 [hep-ph].
 - [20] C.-Y. Seng, X. Feng, M. Gorchtein, and L.-C. Jin, Phys. Rev. D **101**, 111301 (2020), arXiv:2003.11264 [hep-ph].
 - [21] A. Czarnecki, W. J. Marciano, and A. Sirlin, Phys. Rev. D **100**, 073008 (2019), arXiv:1907.06737 [hep-ph].
 - [22] L. Hayen, Phys. Rev. D **103**, 113001 (2021), arXiv:2010.07262 [hep-ph].
 - [23] P.-X. Ma, X. Feng, M. Gorchtein, L.-C. Jin, K.-F. Liu, C.-Y. Seng, B.-G. Wang, and Z.-L. Zhang, Phys. Rev. Lett. **132**, 191901 (2024), arXiv:2308.16755 [hep-lat].
 - [24] W. Jaus and G. Rasche, Phys. Rev. D **41**, 166 (1990).
 - [25] F. C. Barker, B. A. Brown, W. Jaus, and G. Rasche, Nucl. Phys. A **540**, 501 (1992).
 - [26] I. S. Towner, Nucl. Phys. A **540**, 478 (1992).
 - [27] I. S. Towner, Phys. Lett. B **333**, 13 (1994), arXiv:nucl-th/9405031.
 - [28] M. Gorchtein, Phys. Rev. Lett. **123**, 042503 (2019), arXiv:1812.04229 [nucl-th].
 - [29] M. Gorchtein and C. Y. Seng, Ann. Rev. Nucl. Part. Sci.

- 74**, 23 (2024), arXiv:2311.00044 [nucl-th].
- [30] M. Gorchtein and C.-Y. Seng, *Universe* **9**, 422 (2023), arXiv:2307.01145 [hep-ph].
- [31] J. D. Walecka, *Theoretical nuclear and subnuclear physics* (World Scientific, 2004).
- [32] W. Haxton and C. Lunardini, *Computer Physics Communications* **179**, 345 (2008).
- [33] T. Donnelly and W. Haxton, *Atomic Data and Nuclear Data Tables* **23**, 103 (1979).
- [34] C.-Y. Seng and M. Gorchtein, *Phys. Rev. C* **107**, 035503 (2023), arXiv:2211.10214 [nucl-th].
- [35] A. Glick-Magid and D. Gazit, *Journal of Physics G: Nuclear and Particle Physics* **49**, 105105 (2022).
- [36] D. Gazda, R. Catena, and C. Forssén, *Phys. Rev. D* **95**, 103011 (2017).
- [37] A. Glick-Magid, C. Forssén, D. Gazda, D. Gazit, P. Gysbers, and P. Navrátil, *Physics Letters B* **832**, 137259 (2022).
- [38] B. R. Barrett, P. Navrátil, and J. P. Vary, *Prog. Part. Nucl. Phys.* **69**, 131 (2013).
- [39] D. R. Entem, R. Machleidt, and Y. Nosyk, *Phys. Rev. C* **96**, 024004 (2017), arXiv:1703.05454 [nucl-th].
- [40] P. Gysbers, G. Hagen, J. D. Holt, G. R. Jansen, T. D. Morris, P. Navrátil, T. Papenbrock, S. Quaglioni, A. Schwenk, S. R. Stroberg, and K. A. Wendt, *Nature Phys.* **15**, 428–431 (2019).
- [41] K. Kravvaris, P. Navrátil, S. Quaglioni, C. Hebborn, and G. Hupin, *Physics Letters B* **845**, 138156 (2023).
- [42] L. Giralanda, A. Kievsky, and M. Viviani, *Phys. Rev. C* **84**, 014001 (2011), [Erratum: *Phys.Rev.C* **102**, 019903 (2020)], arXiv:1102.4799 [nucl-th].
- [43] S. K. Bogner, R. J. Furnstahl, and R. J. Perry, *Phys. Rev. C* **75**, 061001(R) (2007).
- [44] R. Haydock, *Journal of Physics A: Mathematical, Nuclear and General* **7**, 2120 (1974).
- [45] E. Dagotto, *Rev. Mod. Phys.* **66**, 763 (1994).
- [46] M. Marchisio, N. Barnea, W. Leidemann, and G. Orlandini, *Few-Body Systems* **33**, 259 (2003).
- [47] Y. Hao, P. Navrátil, E. B. Norrgard, M. Iliaš, E. Eliav, R. G. E. Timmermans, V. V. Flambaum, and A. Borschevsky, *Phys. Rev. A* **102**, 052828 (2020).
- [48] P. Froese and P. Navrátil, *Phys. Rev. C* **104**, 025502 (2021).
- [49] R. Haydock, V. Heine, and M. J. Kelly, *Journal of Physics C: Solid State Physics* **5**, 2845 (1972).
- [50] E. Dagotto, *Rev. Mod. Phys.* **66**, 763 (1994).
- [51] D. Bessis and M. Villani, *Journal of Mathematical Physics* **16**, 462 (1975).
- [52] N. Armesto, *J. Phys. G* **32**, R367 (2006), arXiv:hep-ph/0604108.
- [53] B. Z. Kopeliovich, J. G. Morfin, and I. Schmidt, *Prog. Part. Nucl. Phys.* **68**, 314 (2013), arXiv:1208.6541 [hep-ph].
- [54] J. J. Kelly, *Phys. Rev. C* **70**, 068202 (2004).
- [55] J. C. Hardy and I. S. Towner, *Phys. Rev. C* **91**, 025501 (2015), arXiv:1411.5987 [nucl-ex].
- [56] S. Fretwell, K. G. Leach, C. Bray, G. B. Kim, J. Dilling, A. Lennarz, X. Mougeot, F. Ponce, C. Ruiz, J. Stackhouse, and S. Friedrich, *Phys. Rev. Lett.* **125**, 032701 (2020).
- [57] K. G. Leach and S. Friedrich (BeEST), *J. Low Temp. Phys.* **209**, 796 (2022), arXiv:2112.02029 [nucl-ex].
- [58] D. Carney, K. G. Leach, and D. C. Moore, *PRX Quantum* **4**, 010315 (2023), arXiv:2207.05883 [hep-ex].
- [59] O. Nachtmann, *Nucl. Phys. B* **63**, 237 (1973).
- [60] O. Nachtmann, *Nucl. Phys. B* **78**, 455 (1974).
- [61] D. J. Gross and C. H. Llewellyn Smith, *Nucl. Phys.* **B14**, 337 (1969).
- [62] A. L. Kataev and A. V. Sidorov, *Phys. Lett.* **B331**, 179 (1994), arXiv:hep-ph/9402342 [hep-ph].
- [63] J. H. Kim *et al.*, *Phys. Rev. Lett.* **81**, 3595 (1998), arXiv:hep-ex/9808015 [hep-ex].
- [64] S. A. Larin and J. A. M. Vermaseren, *Phys. Lett. B* **259**, 345 (1991).
- [65] P. A. Baikov, K. G. Chetyrkin, and J. H. Kuhn, *Nucl. Phys. B Proc. Suppl.* **205–206**, 237 (2010), arXiv:1007.0478 [hep-ph].
- [66] P. Baikov, K. Chetyrkin, and J. Kuhn, *Phys. Rev. Lett.* **104**, 132004 (2010), arXiv:1001.3606 [hep-ph].
- [67] R. J. Glauber, *Lectures in theoretical physics*, Interscience, New York London (1959).
- [68] V. N. Gribov, *Sov. Phys. JETP* **29**, 483 (1969).
- [69] E. Epelbaum, H. Krebs, and U. G. Meißner, *Eur. Phys. J. A* **51**, 53 (2015), arXiv:1412.0142 [nucl-th].


 Figure S1: The nuclear γW -box diagrams.

SUPPLEMENTARY MATERIAL

This supplementary material collects information not displayed in the core manuscript that falls into one of the following categories:

- It is available in the quoted references and is reproduced for the reader's convenience
- It involves technical details of the *ab initio* calculation which do not alter the main discussions
- It is needed for a complete analysis of the δ_{NS} uncertainties, but is independent of the *ab initio* calculation

Terms in the nuclear box diagram

Here we provide the analytic expressions for the three terms on the right-hand-side of Eq. (5) which stem from the nuclear γW -box diagram in Fig. S1; approximate forms have been previously derived in Refs. [29, 34] but generalized here to retain the full E_e - and m_e -dependence.

First, the Wick-rotated term reads

$$\begin{aligned}
 (\square_{\gamma W}^b)_{\text{Wick}}(E_e) &= -\frac{\alpha}{\pi M} \int_0^\infty d\mathbf{q} \mathbf{q}^2 \int_{-\infty}^\infty \frac{d\nu_E}{2\pi} \frac{M_W^2}{M_W^2 + Q^2} \\
 &\times \frac{1}{Q^2} \frac{T_3(i\nu_E, \mathbf{q})}{f_{+\nu_E}} \left\{ \frac{2(\mathbf{p}_e^2 \mathbf{q}^2 + E_e^2 \nu_E^2) - iQ^2 \nu_E E_e}{4\mathbf{p}_e^3 \mathbf{q}} \right. \\
 &\times \ln \left(\frac{-2iE_e \nu_E - Q^2 + 2\mathbf{p}_e \mathbf{q}}{-2iE_e \nu_E - Q^2 - 2\mathbf{p}_e \mathbf{q}} \right) - \frac{i\nu_E E_e}{\mathbf{p}_e^2} \left. \right\}, \quad (\text{S1})
 \end{aligned}$$

where $\mathbf{p}_e = |\vec{p}_e|$ and $Q^2 = \nu_E^2 + \mathbf{q}^2$. Next, the residue contribution from the electron propagator reads

$$\begin{aligned}
 (\square_{\gamma W}^b)_{\text{res},e}(E_e) &= \frac{i\alpha}{2\pi M} \int_0^{2\mathbf{p}_e} d\mathbf{q} \mathbf{q}^2 \int_{\mathbf{q}/2\mathbf{p}_e}^1 dx \frac{1}{\nu_e^2 - \mathbf{q}^2} \\
 &\times \frac{\frac{\nu_e \mathbf{q} E_e x - \mathbf{q}^2}{\mathbf{p}_e}}{\sqrt{E_e^2 - 2\mathbf{p}_e \mathbf{q} x + \mathbf{q}^2}} \frac{T_3(\nu_e, \mathbf{q})}{f_{+\nu_e}}, \quad (\text{S2})
 \end{aligned}$$

where

$$\nu_e = E_e - \sqrt{E_e^2 - 2\mathbf{p}_e \mathbf{q} x + \mathbf{q}^2}. \quad (\text{S3})$$

Adding Eqs. (S1), (S2) and expanding the result in powers of E_e (in the $m_e = 0$ limit) yields

$$\begin{aligned}
 (\square_{\gamma W})_{\text{Wick}}(E_e) + (\square_{\gamma W})_{\text{res},e}(E_e) \\
 = \Xi_0 + \Xi_1 E_e + \mathcal{O}(E_e^2), \quad (\text{S4})
 \end{aligned}$$

where the coefficients $\Xi_{0,1}$ may be found in Ref.[29]. We note that, while convenient, such expansion is not necessary. Finally, the residue contribution from the Compton amplitude T_3 due to a given state k in the low-lying nuclear spectrum of ^{10}B reads

$$\begin{aligned}
 (\square_{\gamma W}^b)_{\text{res},T_3} &= \frac{i\alpha}{\pi M} \int_0^{\mathbf{q}_{\text{max}}} d\mathbf{q} \mathbf{q}^2 \frac{\text{Res } T_3(\nu_k, \mathbf{q})}{f_+} \\
 &\times \frac{1}{\mathbf{q}^2 - \nu_k^2} \left\{ \frac{2\mathbf{p}_e^2 \mathbf{q}^2 + \nu_k E_e (\nu_k^2 - 2E_e \nu_k - \mathbf{q}^2)}{4\nu_k \mathbf{p}_e^3 \mathbf{q}} \right. \\
 &\times \ln \left[\frac{\nu_k^2 - 2E_e \nu_k - \mathbf{q}^2 + 2\mathbf{p}_e \mathbf{q}}{\nu_k^2 - 2E_e \nu_k - \mathbf{q}^2 - 2\mathbf{p}_e \mathbf{q}} \right] - \frac{E_e}{\mathbf{p}_e^2} \left. \right\}, \quad (\text{S5})
 \end{aligned}$$

where

$$\text{Res } T_3(\nu_k, \mathbf{q}) = \lim_{\nu \rightarrow \nu_k} (\nu - \nu_k) T_3(\nu, \mathbf{q}), \quad (\text{S6})$$

with

$$\nu_k(\mathbf{q}) = M_k - M_f + \frac{\mathbf{q}^2}{2M_k}, \quad (\text{S7})$$

and

$$\mathbf{q}_{\text{max}} = \sqrt{M_f^2 - M_k^2}. \quad (\text{S8})$$

Multipole expansion and dependence on nucleon form factors

Connection of the SM currents appearing in the Compton amplitude in Eq. (3) to the effective nucleon-level one-body operators compatible with nuclear many-body theory is accomplished via the tried and true multipole expansion formalism. Comprehensive reviews on the topic may be found in Refs. [31–33]. For the reader’s convenience, we quote the definition of the relevant nucleonic operators appearing in Eq. (4).

$$T_{JM_J}^{\text{el}}(\mathbf{q}\mathbf{x}) \quad (\text{S 9})$$

$$= \frac{\mathbf{q}}{M_N} \left\{ F_1(q^2) \Delta'_{JM_J}(\mathbf{q}\mathbf{x}) + \frac{1}{2} \mu(q^2) \Sigma_{JM_J}(\mathbf{q}\mathbf{x}) \right\}$$

$$iT_{JM_J}^{\text{mag}}(\mathbf{q}\mathbf{x}) \quad (\text{S 10})$$

$$= \frac{\mathbf{q}}{M_N} \left\{ F_1(q^2) \Delta_{JM_J}(\mathbf{q}\mathbf{x}) - \frac{1}{2} \mu(q^2) \Sigma'_{JM_J}(\mathbf{q}\mathbf{x}) \right\}$$

$$iT_{JM_J}^{5,\text{el}}(\mathbf{q}\mathbf{x}) = -F_A \Sigma'_{JM_J}(\mathbf{q}\mathbf{x}) \quad (\text{S 11})$$

$$iT_{JM_J}^{5,\text{mag}}(\mathbf{q}\mathbf{x}) = F_A \Sigma_{JM_J}(\mathbf{q}\mathbf{x}) \quad (\text{S 12})$$

We are consistent with the form factor independent electroweak operator basis defined in Ref. [33] which assumes the vanishing nature of second-class currents. The combination of the form factor independent pieces into the full multipole operators is accomplished by applying the dipole form of the single-nucleon form factors; discussion pertaining to the error attributed to this choice is discussed in the following sections.

The nuclear shadowing effect

Here we display some details from which we obtain Eq. (7) and the subsequent estimation of the nuclear shadowing uncertainty.

As pointed in the manuscript, the full nuclear box diagram $\square_{\gamma W}^{b,\text{nuc}}$ appearing in Eq. (2) includes contributions from all intermediate states, both nucleonic and non-nucleonic. However, the piece that we compute with *ab initio* nuclear theory, $(\square_{\gamma W}^{b,\text{nuc}})_{\text{a.i.}}$, covers only the nucleonic contributions. Information of non-nucleonic intermediate states is available from the single-nucleon box diagram, which splits into the elastic and inelastic piece:

$$\square_{\gamma W}^{b,n} = (\square_{\gamma W}^{b,n})_{\text{el}} + (\square_{\gamma W}^{b,n})_{\text{inel}}, \quad (\text{S 13})$$

where $(\square_{\gamma W}^{b,n})_{\text{el}} = 0.106(6) \times 10^{-3}$ and $(\square_{\gamma W}^{b,n})_{\text{inel}} = 0.054(6) \times 10^{-3}$ after averaging over results from several dispersion relation analysis [30]. Note that we do not include the result from the recent lattice calculation

of $\square_{\gamma W}^{b,n}$ [23] because the separation above was not performed.

The non-nucleonic intermediate state contributions to the single-nucleon box diagram are contained entirely in $(\square_{\gamma W}^{b,n})_{\text{inel}}$, which can be used to reconstruct the missing piece in $\square_{\gamma W}^{b,\text{nuc}}$. A first attempt is to postulate:

$$\square_{\gamma W}^{b,\text{nuc}} \stackrel{?}{=} (\square_{\gamma W}^{b,\text{nuc}})_{\text{a.i.}} + (\square_{\gamma W}^{b,n})_{\text{inel}}, \quad (\text{S 14})$$

which is, of course, not entirely rigorous because $(\square_{\gamma W}^{b,n})_{\text{inel}}$ is modified in a nuclear medium:

$$(\square_{\gamma W}^{b,n})_{\text{inel}} \rightarrow (\square_{\gamma W}^{b,n})_{\text{inel}} + \delta(\square_{\gamma W}^{b,n})_{\text{sh}}, \quad (\text{S 15})$$

where the modification $\delta(\square_{\gamma W}^{b,n})_{\text{sh}}$ is not calculable using *ab initio* methods. Our goal is to estimate an upper limit of its size which is to be included in the theoretical uncertainty of δ_{NS} .

In the dispersive representation (with $E_e \rightarrow 0$), one can express the box diagram as [19]

$$\square_{\gamma W}^b = \frac{3\alpha}{2\pi} \int_0^\infty \frac{dQ^2}{Q^2} \frac{M_W^2}{M_W^2 + Q^2} M_3(Q^2), \quad (\text{S 16})$$

where $M_3(Q^2)$ is the “first Nachtmann moment” [59, 60] of a parity-odd structure function $F_3(x, Q^2)$, which involves its integral with respect to the Bjorken variable x . So, to understand $\delta(\square_{\gamma W}^{b,n})_{\text{sh}}$ we need to know the size of nuclear modifications to $M_3(Q^2)$ as a function of Q^2 . It is known that, with increasing Bjorken variable x the nuclear modification to a structure function exhibits an oscillatory behavior from shadowing to anti-shadowing [52], which effects partially cancel in the moments. In fact, as far as the parity-odd nuclear structure function F_3^{nuc} (which is responsible for $(\square_{\gamma W}^{b,n})_{\text{inel}}$) is concerned, the good agreement between the experimentally-determined Gross-Llewellyn Smith (GLS) sum rule [61] on iron target [62, 63] and theory prediction to $\mathcal{O}(\alpha_s^4)$ [64–66] indicates that its first Nachtmann moment is not affected by shadowing in the deep inelastic region ($Q^2 > 2 \text{ GeV}^2$). For $Q^2 < 2 \text{ GeV}^2$, we may gain some insights on the size of nuclear shadowing using data from the parity-even structure function F_2^{nuc} . From ${}^9\text{Be}$ to ${}^{12}\text{C}$, the upper bound of nuclear modifications varies between 10% and 20% (see, e.g. Figs. 22, 51 of Ref. [53] and references therein). Therefore, we may take the result of the inelastic single-nucleon box diagram at $Q^2 < 2 \text{ GeV}^2$: $(\square_{\gamma W}^{b,n})_{\text{inel}}(Q^2 < 2 \text{ GeV}^2) \approx 0.59 \times 10^{-3}$ [30] and multiply it by 20% as a conservative estimation of the nuclear shadowing uncertainty in $\square_{\gamma W}^{\text{nuc}}$. The prescription above translates into the following relation:

$$\square_{\gamma W}^{b,\text{nuc}} = (\square_{\gamma W}^{b,\text{nuc}})_{\text{a.i.}} + \left\{ (\square_{\gamma W}^{b,n})_{\text{inel}} + \delta(\square_{\gamma W}^{b,n})_{\text{sh}} \right\}, \quad (\text{S 17})$$

or, in terms of δ_{NS} ,

$$\begin{aligned}\delta_{\text{NS}} &= 2(\square_{\gamma W}^{b,\text{nuc.}} - \square_{\gamma W}^{b,n}) \\ &= 2 \left\{ (\square_{\gamma W}^{b,\text{nuc.}})_{\text{a.i.}} - (\square_{\gamma W}^{b,n})_{\text{el}} + \delta(\square_{\gamma W}^{b,n})_{\text{sh}} \right\}\end{aligned}\quad (\text{S } 18)$$

which is just Eq. (7), with

$$\begin{aligned}|\delta(\square_{\gamma W}^{b,n})_{\text{sh}}| &< 0.2 \times (\square_{\gamma W}^{b,n})_{\text{inel}}(Q^2 < 2\text{GeV}^2) \\ &\approx 1.2 \times 10^{-4}.\end{aligned}\quad (\text{S } 19)$$

Some of the implicit assumptions in the treatment above, for example the similarity between the shadowing effects to P-even and P-odd structure functions, should be scrutinized with in-depth theoretical study using, e.g., the Glauber-Gribov approach [67, 68]. This will be performed in a future work.

Detailed error analysis

In this section we provide the finer details regarding the various nuclear modelling errors entering into the evaluations given in Fig. 4 as well as Eqs. (8) and (9), sans the nuclear shadowing effects which have been thoroughly explored in the previous section. A precise summary of the error breakdown is provided in Table. SI.

First and foremost, due to the computational complexity of nuclear many-body calculations we encounter three types of truncation in these calculations: (i) the truncation of the many-body HO basis in the NCSM, controlled by the parameter N_{max} (ii) the truncation of the multipole expansion, controlled by the parameter J_{max} and (iii) the truncation of the chiral expansion. As N_{max} controls the many-body basis size, in the limit $N_{\text{max}} \rightarrow \infty$ we approach the exact NCSM result. At finite N_{max} , we estimate the truncation error $\epsilon_{N_{\text{max}}}$ by taking the absolute difference of consecutive N_{max} evaluations of δ_{NS} . In addition, we use the residual dependence on the HO frequency Ω to estimate the error incurred, ϵ_{Ω} , by choosing the frequency $\hbar\Omega = 18$ MeV when evaluating δ_{NS} . It is estimated by taking the maximum absolute difference between varied frequency calculations in the vicinity of $\hbar\Omega = 18$ MeV. On the other hand, the multipole contributions are observed to be oscillating in sign and decreasing in absolute value. We thus estimate the associated error, $\epsilon_{J_{\text{max}}}$, by taking the absolute magnitude of the last multipole contribution, i.e., at $J_{\text{max}} = 3$. Lastly, the truncation of the chiral expansion introduces an error ϵ_{χ} . A well motivated approach to the estimation of chiral interaction uncertainties at the many-body level is discussed in Ref. [69] and applied in Ref. [41] with the

NCSM. It involves fully consistent calculations at each order in the chiral expansion which, purely as a result of the cost of these calculations, we are not able to perform. Instead, we may still reasonably estimate the effects of the truncation by varying the chiral interaction in use. To this end, we have considered the so-called E_7 interaction which includes an additional sub-leading contact interaction in the three-nucleon sector. The final result is taken as the average of those two calculations and its dispersion is used as the additional uncertainty ϵ_{χ} . These characterize all truncation uncertainties entering the *ab initio* many-body calculation of δ_{NS} .

Next to be discussed is the treatment of the 4-momentum dependence of the electroweak currents. As discussed in a previous section, those are decomposed in an operator basis and second-class currents are assumed to be vanishing [33]. The only model dependence left consists of the 4-momentum dependence of the form factors that we use for electromagnetic and weak processes. For a general form factor appearing in Eqs. (S9) – (S12), we use the standard dipole form factor approximation

$$F(q^2) = F(0) \left[1 + \frac{q^2}{M_{\text{scale}}^2} \right]^{-2}, \quad (\text{S } 20)$$

where in this context M_{scale} refers to either the vector dipole mass M_V or the axial dipole mass M_A . This approximation is uncontrolled in the sense that it is merely recognized as a convenient fitting procedure for a given form factor's momentum distribution. Nevertheless, we can conservatively estimate the error arising from such an approximation by varying the corresponding dipole mass to span the entire range of more sophisticated form factor fitted to reproduce experimental data. Proceeding in this way, the vector dipole mass is varied in a range of 800 – 1000 MeV to cover the range of predictions from the high-quality Padé fits performed in Ref. [54] whereas the axial dipole mass is varied in a range of 1.09 – 1.270 GeV as recommended in Ref. [18]. Combined with the N_{max} truncation error and multipole truncation error, this makes up the partial model errors given in Table. SI.

At the moment, the errors discussed in this section represent the largest contributions to the uncertainty in the δ_{NS} prediction. Future systematic improvements to the formalism are envisioned, for example, improvements to the theoretical calculation of δ_{NS} could be achieved by inclusion of higher-body currents and relativistic corrections or simply by using a more precise extractions of form factors. Finally, let us mention that most of the developments discussed here can be extended to other electroweak radiative corrections.

$^{10}\text{C} \rightarrow ^{10}\text{B}$	This work	Ref. [17]	$\times 10^{-4}$
$\epsilon_{J_{\max}}$	0.83	3.3	$\epsilon_{\delta_{\text{NS},A}}$
$\epsilon_{M_{\text{scale}}}$	0.036	3.5	$\epsilon_{\delta_{\text{NS},B}}$
$\epsilon_{N_{\max}}$	0.60	1.5	$\epsilon_{\delta_{\text{NS},E}}$
ϵ_{PME}	1.0	/	
ϵ_{Ω}	0.8	/	
ϵ_{χ}	1.0	/	
ϵ_{sh}	2.4	/	
ϵ_{nuc}	2.9	/	
$\epsilon_{n,\text{el}}$	1.2	/	
$\epsilon_{\delta_{\text{NS}}}$	3.1	5.0	$\epsilon_{\delta_{\text{NS}}}$

Table S I: List of different uncertainties accounted for in the δ_{NS} calculation discussed in this Letter. For comparison, we also provide the uncertainties considered in Ref. [17]. Different sub-groups correspond to different degree of aggregation of the uncertainties.